Cloud Resolving Simulations of Mixed-Phase Arctic Stratus Observed during BASE: Sensitivity to Concentration of Ice Crystals and Large-Scale Heat and Moisture Advection

HONGLI JIANG AND WILLIAM R. COTTON

Department of Atmospheric Science, Colorado State University, Fort Collins, Colorado

JAMES O. PINTO AND JUDY A. CURRY

Program in Atmospheric and Oceanic Sciences, University of Colorado, Boulder, Colorado

MICHAEL J. WEISSBLUTH

Mission Research Corporation, Aster Division, Fort Collins, Colorado

(Manuscript received 3 August 1998, in final form 28 July 1999)

ABSTRACT

The authors' previous idealized, two-dimensional cloud resolving model (CRM) simulations of Arctic stratus revealed a surprising sensitivity to the concentrations of ice crystals. In this paper, simulations of an actual case study observed during the Beaufort and Arctic Seas Experiment are performed and the results are compared to the observed data.

It is again found in the CRM simulations that the simulated stratus cloud is very sensitive to the concentration of ice crystals. Using midlatitude estimates of the availability of ice forming nuclei (IFN) in the model, the authors find that the concentrations of ice crystals are large enough to result in the almost complete dissipation of otherwise solid, optically thick stratus layers. A tenuous stratus can be maintained in the simulation when the continuous input of moisture through the imposed large-scale advection is strong enough to balance the ice production. However, in association with the large-scale moisture and warm advection, only by reducing the concentration of IFN to 0.3 of the midlatitude estimate values can a persistent, optically thick stratus layer be maintained. The results obtained from the reduced IFN simulation compare reasonably well with observations.

The longwave radiative fluxes at the surface are significantly different between the solid stratus and liquid-water-depleted higher ice crystal concentration experiments.

This work suggests that transition-season Arctic stratus can be very vulnerable to anthropogenic sources of IFN, which can alter cloud structure sufficiently to affect the rates of melting and freezing of the Arctic Ocean.

The authors find that the Hallett–Mossop riming splintering mechanism is not activated in the simulations because the cloud droplets are very small and cloud temperatures are outside the range supporting efficient rime splintering. Thus, the conclusions drawn from the results presented in this paper may be applicable to only a limited class of Arctic stratus.

1. Introduction

Considerable interest in Arctic clouds has been generated by the growing awareness of the sensitivity of Arctic climate to global warming and the importance of the surface radiation budget in determining the sea–ice mass balance (for a review, see Curry et al. 1996). Among the several unusual boundary layer cloud types that have been observed in the Arctic (Curry et al. 1996),

the mixed-phase clouds that occur in the Arctic boundary layer during the spring have been identified as a programmatic focus for the National Aeronautics and Space Administration First International Satellite Cloud Climatology Project (ISCCP) Regional Experiment III Arctic Clouds Experiment (Curry et al. 1998, manuscript submitted to *Bull. Amer. Meteor. Soc.*). A motivation for this focus is provided by the modeling results of Curry and Ebert (1992), who inferred a 50% decrease in cloud optical depth associated with the transition of low-level clouds from predominately liquid to ice. The importance of correctly simulating mixed-phase clouds in global climate models has been emphasized by Gregory and Morris (1996).

During the autumn of 1994, the Beaufort Arctic

Corresponding author address: Hongli Jiang, Department of Atmospheric Science, Colorado State University, Fort Collins, CO 80523.
E-mail: jiang@atmos.colostate.edu

Storms Experiment (BASE) was conducted in the Beaufort Sea (Curry et al. 1997). Among the cases obtained from the National Center for Atmospheric Research C-130 research aircraft were two cases of mixed-phase boundary layer clouds (Pinto 1998; hereafter P98). It should be noted here that the cloudy boundary layer is loosely defined as lower-level stratus cloud layers within, atop, or directly influencing the vertical structure of the atmospheric boundary layer (see Curry et al. 1988).

Mixed-phase clouds are commonly observed but difficult to simulate because of their colloidal instability, especially in winter arctic stratus. The cases described by P98 remained as mixed-phase clouds over the course of several hours of aircraft measurements. P98 hypothesized that the clouds were maintained as mixed phase by continued production of liquid water by cloud-top cooling, and the maintenance of the mixed-phase cloud was highly dependent on the ice nucleation rate determined by the ice forming nucleus (IFN) concentration.

Evidence for small values of IFN in the Arctic is provided by the observations of Bigg (1996), who found mean IFN concentrations ranging from 0.013 to 0.0029 L^{-1} at $-15°C$ during a voyage to the North Pole in the fall of 1991. These IFN values are considerably smaller than estimates of IFN activation by deposition nucleation derived from continuous flow diffusion measurements in midlatitudes (Meyers et al. 1992; hereafter M92). The composition of IFN observed (or inferred) in the Arctic include clay and related minerals (Kumai and Francis 1962); pollution aerosol (Borys 1989), and biogenic nuclei from the ocean (Schnell 1977; Bigg 1996).

In a recent numerical modeling study of arctic stratocumulus cloud, Harrington et al. (1999; hereafter H99) simulated transition-season stratus clouds by simply reducing the initial θ values from the sounding taken during the 28 June 1980 period of the Arctic stratus experiment by 5° and 10°C, resulting in temperatures at the lowest model level as between $-16°$ and $-20.8°C$, respectively. The cooling resulted in a mixed-phase stratus that resembled many features of the mixed-phase clouds observed during BASE. Sensitivity experiments performed by H99 revealed that a mixed-phase, well-mixed stratus layer cloud can be maintained if ice crystal concentrations did not exceed 2 L^{-1} in the 5°C cooling simulation and 0.4 L^{-1} in the 10°C cooling simulation.

In this paper, we extend the simulations of H99 and use a cloud resolving model to examine one of the cases of arctic mixed-phase boundary layer clouds described by P98. Sensitivity studies are conducted to examine the influence of variable concentrations of ice crystals on cloud microphysics, boundary layer structure, and the surface energy budget. We also evaluate the role of large-scale advective tendencies of temperature and moisture on the maintenance of the mixed-phase cloud.

It should be noted that the clouds described in P98 and simulated in this study are not representative of all stratocumulus clouds observed in the Arctic. The clouds observed during BASE tend to have smaller liquid particle sizes and colder temperatures ($-18°$ to $-20°C$) than those observed in June 1995 over the Beaufort Sea by Hobbs and Rangno (1998; hereafter HR98), but have characteristics similar to a number of cases observed in April 1992, when the atmosphere is much colder. Because the clouds observed during BASE lacked properties necessary for the Hallett–Mossop (H–M) riming–splintering mechanism to take place, this process is neglected in this study. In addition, the smaller liquid droplets (5–8 μm in diameter) are not likely to grow to drizzle sizes under very low liquid water contents. Therefore, the results and conclusions presented in this study are applicable to those stratocumulus clouds in which neither secondary ice particle production processes (the H–M process) nor precipitation production by collision–coalescence process operate efficiently.

2. Model description and experiment setup

The model used in this study is the two-dimensional (2D) cloud resolving model version of the Regional Atmospheric Modeling System (RAMS) developed at Colorado State University (CSU) (Stevens et al. 1998; H99) combined with the single-moment bulk microphysical parameterization of Walko et al. (1995). This model is the same as the dynamic model used in H99 (without the explicit bin-resolving microphysics) except that a different subgrid-scale model is used (Kosovic 1997) and large-scale advective tendencies of potential temperature and water vapor are imposed for this study. A brief description of the subgrid model will be given in the following. It was found that the dynamic model was able to replicate most of features produced with the bin-resolving microphysics, but with at least two orders of magnitude less model integration time (J. Y. Harrington 1998, personal communication).

The model predicts the wind components (u and w in the 2D framework), the Exner function (π), the ice–liquid water potential temperature (θ_{il}; Tripoli and Cotton 1981), and total water mixing ratio (q_t). In the single-moment bulk microphysical framework (Walko et al. 1995) it is assumed that the hydrometeor size spectra have a gamma distribution function, and only the mass mixing ratio of the hydrometeor species is predicted. The predicted microphysical categories include the mixing ratio of rain, pristine ice, snow,[1] aggregates, graupel, and hail, with cloud liquid water being diagnosed. The number concentration of pristine ice crystals is also predicted.

Ice nucleation by deposition and condensation–freezing is represented in a single empirically based param-

---

[1] Snow is defined here as larger pristine ice crystals which have grown by vapor deposition and riming. Aggregates are defined as ice particles that have formed by collision and coalescence of pristine ice, snow, and/or other aggregates.

eterization described by Meyers et al. (1992). This formulation was derived from the available measurements with continuous flow diffusion chambers in midlatitudes. The parameterization is given by

$$(N_t)_d = \exp(-0.639 + 12.96 r_{si}), \qquad (2.1)$$

where $(N_t)_d$ is the number of nucleated crystals per liter and r_{si} is the supersaturation with respect to ice. This parameterization (or ice-nucleation process) is activated when the ambient water vapor mixing ratio exceeds saturation over ice, and the temperature is below $-5°C$. Because the deposition and condensation-freezing processes could not be separated in the experimental setup, the more conservative $-5°C$ threshold is used to activate the parameterization even though condensation freezing itself could occur as warm as $-2°C$.

A two-stream radiative transfer model is utilized for this study (H99). The two-stream model solves the equation of transfer for three gaseous constituents, H_2O, O_3, and CO_2, which include climatological mixing ratio of CH_4, O_2, and NO_2. Gaseous absorption is calculated by following the fast exponential sum-fitting of transmissions method proposed by Ritter and Geleyn (1992). Lorenz–Mie theory is used to compute the optical properties for water drops, while the theory of Mitchell et al. (1996) is used for nonspherical ice crystals. For each hydrometeor species, the band-averaged values of optical properties are computed for the assumed gamma distribution function used in RAMS following the method of Slingo and Schrecker (1982).

A nonlinear subgrid-scale (SGS) model is used for this study (Kosovic 1997). Unlike a linear-type SGS model (e.g., Smagorinsky 1963), the nonlinear SGS model handles the effects of backscatter of energy as well as normal stress in sheared flows. It is based on previous work associated with the SGS parameterization with improvement in prediction of the low-order statistics and nondimensional shear.

The lateral boundary conditions are cyclic. The boundary condition at the model top corresponds to a rigid lid. In order to minimize spurious reflection of upward-propagating gravity waves, a Rayleigh friction absorbing layer is applied to the momentum equations and thermodynamic equation over the top five levels of the model with damping timescale $\tau = 200$ s (Louis 1979). The bottom boundary is specified to be consistent with surface conditions observed during BASE, with a specified surface temperature of 259.45 K and surface roughness of 0.04 m.

Simulations are done in a two-dimensional (2D) framework. The 2D simulation has a domain of 60 $\times$ 64 grid with a 60-m grid spacing in the horizontal and 30-m grid spacing in the vertical from the surface up to 1500 m, thereafter stretched to 100 m near the domain top (2300 m). The domain is thus 3600 m in the horizontal, and 2300 m in the vertical. A time step of 2 s is used in all integrations. In a comparative study of radiatively driven stratocumulus-topped PBL, Stevens

TABLE 1. Summary of case characteristics.

Flight	Date	Time UTC	Location N, W	Solar zenith angle
18.1	25 Oct 1994	2030	76.8°, 138.8°	89.3°
18.4	25 Oct 1994	2359	76.6°, 138.0°	89.3°

et al. (1996) demonstrated that two-dimensional simulations were able to capture many of the elements of the three-dimensional simulations except the differences between the timescales and structure of boundary layer eddies. Nonetheless, the combination of limited computer resources and shorter integration time makes the use of the 2D framework advantageous over 3D. It should be noted that considering the emerging evidence of highly inhomogeneous ice particle concentrations in clouds, the structure and timescale of eddies within the cloud can be important factors in ice formation. This is not a point to be addressed in this paper, but rather a suggestion for later studies.

3. Case description and model initiation

We simulate one of the cases (case 18.1, P98) of Arctic mixed-phase boundary layer clouds described by P98. The case is characterized by a well-mixed layer (constant θ) with strong potential temperature and moisture inversions both below and above the mixed layer. A low-level jet is also present in the observation. A deep well-mixed layer is present through and beneath the cloud layer, indicating that the turbulence field is relatively well developed and is close to steady state. The inversion layer between 300 and 450 m decouples the cloud layer from the surface, effectively cutting off the surface as a moisture source.

In Table 1 we present the characteristics of case 18.1, including the location, date and time, and solar zenith angle. Note that information for case 18.4 is also listed for later comparison purposes.

The large-scale advective tendencies of potential temperature ($d\theta/dt$) and water vapor (dq_v/dt) are estimated from National Centers for Environmental Prediction (NCEP) reanalysis at six pressure levels (Fig. 4, P98), and horizontally averaged over a $5° \times 5°$ grid box with the location of aircraft at the central point at each pressure level. Owing to the limited number of soundings available in the Arctic, this is a very crude estimate. It should be noted that the NCEP data contain large variations ranging from -2.0 to 3.5 g kg^{-1} day^{-1} in dq/dt and from -5.0 to 14 K day^{-1} in $d\theta/dt$ over an area of $15° \times 15°$ at 925-mb pressure level and a similar range of variations at other pressure levels. Because of the large uncertainty associated with large-scale advection, we explore the importance of potential errors associated with these estimates using sensitivity experiments. The large-scale tendencies are then vertically interpolated to the model's grid and imposed throughout the simulation
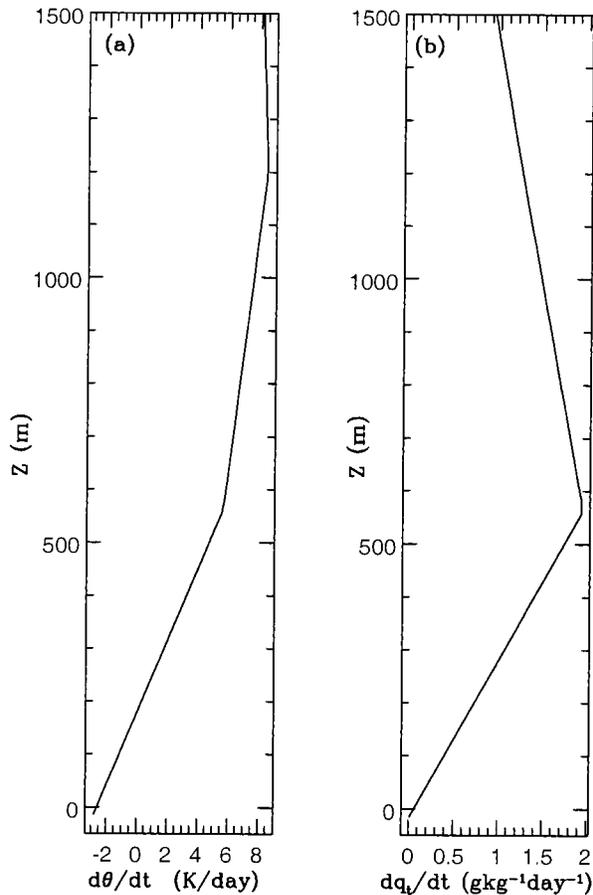
FIG. 1. Vertical profiles of the prescribed large-scale advective tendencies of (a) potential temperature and (b) water vapor.
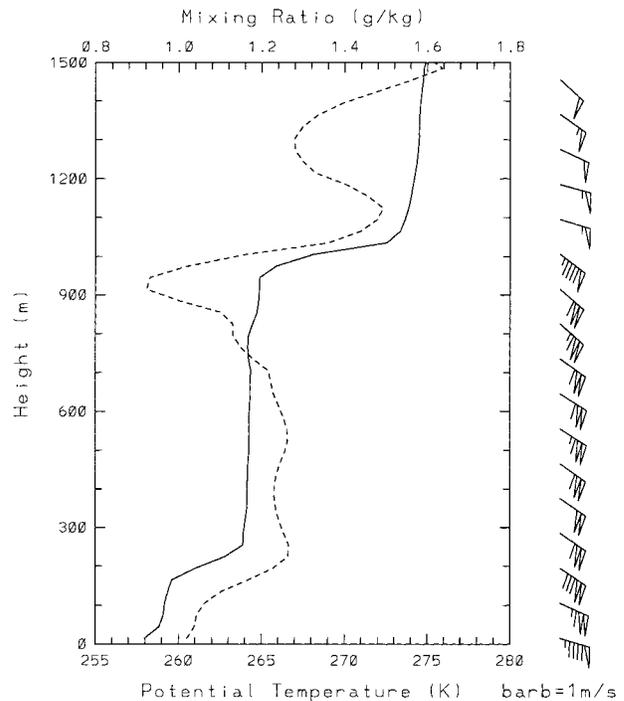

FIG. 2. Vertical profiles of the initial conditions: dry potential temperature (solid line, using bottom label), total water mixing ratio (dashed line, using top label), and wind speed with 1 m s^{-1} wind barb.

(Fig. 1). Note that there is cold advection below 200 m and warm advection above (Fig. 1a), while there is moisture advection throughout the entire domain (Fig. 1b). The NCEP reanalysis relative to advection patterns are supported by the sounding profiles for this day.

The model is initialized with horizontally uniform fields, so a random perturbation of 0.2 K maximum magnitude in the potential temperature field is imposed in the lowest several model levels at the first time step to create an initial inhomogeneity. The initial dry potential temperature θ and total water mixing ratio q_t profiles and wind barbs are taken from 18.1 in P98 and given in Fig. 2. The observed instantaneous profiles of θ and q_t (not shown) consists of four layers: A surface-based mixed layer, an inversion layer between 300 and 450 m, a cloud-topped mixed layer, and a capping inversion layer. The fields shown in Fig. 2 have a slightly different representation that was obtained from the observed mean profile. Nevertheless, a very strong inversion with a 9 K increase in θ and 0.5 g kg^{-1} increase in q_t is present at cloud top (1000 m). The initial wind is primarily from the southeast below cloud top with a sharp decrease in wind speed at the inversion. Note that

a low-level jet ($|U| = 13.0$ m s^{-1}) with its core around 200 m is present.

Simulations are done in two steps. A 1-h spinup is performed without the bulk microphysics parameterization in order to produce the initial cloud rapidly and establish the resolved-scale turbulence. During the spinup period, the model allows condensation to occur whenever supersaturation is attained. The partitioning of the total water substance into vapor and cloud liquid water is diagnostic. No other forms of liquid or ice water are considered. The large-scale advective tendencies are imposed during the spinup period with the magnitudes of twice the NCEP value. An additional hour of simulation is done with the bulk microphysics after the spinup time.

4. Simulation results—Sensitivity experiments

Sensitivity experiments are performed in the second hour of simulation after the spinup with the bulk microphysics. Special focus in the sensitivity experiments is on the concentration of ice crystals and their ability to deplete liquid water content. Because the ice crystal concentrations for this case are largely controlled by IFN concentrations, variations of ice crystal concentrations are realized by varying concentrations of IFN. The conditions for optimum secondary production of ice droplets by the Hallett–Mossop (Mossop 1985) rime–splinter mechanism are not met for this case.

TABLE 2. Description of experiments.

	Microphysics	IFN	L–S advection
Spinup	no		2.0[a] NCEP[c]
I1-A1	yes	1.0[a] M92[b]	1.0[a] NCEP
I1-A2	yes	1.0[a] M92	2.0[a] NCEP
I1-A3	yes	1.0[a] M92	3.0[a] NCEP
I1-A4	yes	1.0[a] M92	4.0[a] NCEP
I3/10-A2	yes	0.3[a] M92	2.0[a] NCEP
I1/10-A2	yes	0.1[a] M92	2.0[a] NCEP
I3/10-A3	yes	0.3[a] M92	3.0[a] NCEP

[a] See text for details.
[b] Use original IN value from Meyers et al. (1992).
[c] Use twice of the NCEP value.

Our baseline simulation is done with the number concentration of IFN estimated from midlatitude values (M92) and the large-scale advection terms of NCEP reanalysis values (hereafter refer to this simulation as I1-A1). The sensitivity to large-scale advection is done by keeping the number concentration of IFN as in I1-A1, while increasing the imposed large-scale advective tendencies of potential temperature and water vapor to twice (hereafter as I1-A2), three times (hereafter as I1-A3), and four times (hereafter as I1-A4) of that shown in Fig. 1. The sensitivity to the concentration of ice crystals is examined by reducing the IFN concentration used in I1-A2 to 0.1 and 0.3 of its value, respectively, while all other elements of the model remain the same as in I1-A2 (hereafter as I1/10-A2 and I3/10-A2, respectively). A realistic simulation of mixed-phase stratus cloud is achieved when the combination of reducing the IFN to 0.3 of that estimated from midlatitude values and increasing the large-scale advective tendency to three time of that NCEP reanalysis values (hereafter as I3/10-A3) is used. The experiments are summarized in Table 2.

a. Sensitivity to concentration of IFN

P98 inferred from observations and a simple microphysical model that depleted IFN allowed for low-level clouds to remain mixed phase for extended periods of time. To test this hypothesis the number concentration of IFN are reduced from estimated midlatitude values (M92) to determine the influence of ice crystal concentration on the stability of mixed-phase clouds.

The time variability of cloud liquid water path (LWP), ice water path (IWP),[2] and snow water path (SWP), is plotted for the I1-A2, I3/10-A2, I1/10-A2, and I3/10-A3 runs to examine the microphysical response of the simulated stratus cloud to the changes in IFN concentration as well as large-scale advection (Fig. 3). Com-

---

[2] The ice category is defined as pristine ice only, while snow consists of aggregates, graupel, and snow in the calculation for all the runs.
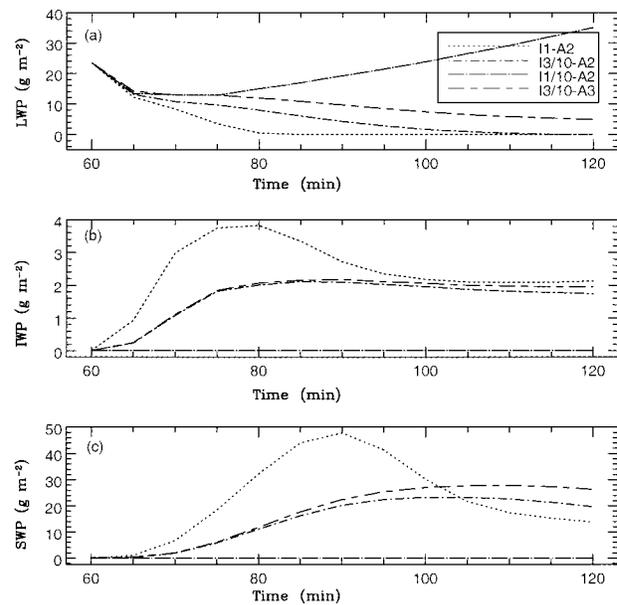

FIG. 3. Time evolution of domain-averaged (a) cloud liquid water path (LWP) (g m^{-2}), (b) ice water path (IWP) (g m^{-2}), and (c) snow water path (SWP) (g m^{-2}) for the I1-A2, I3/10-A2, I1/10-A2, and I3/10-A3 runs. See Table 2 for definitions.

parison among these runs shows that a realistic simulation with a sustained, mixed-phase stratus cloud is produced for the entire second hour of simulation when the IFN concentration is reduced to 0.3 of its original value estimated for midlatitudes (M92) while the advective tendencies are three times the NCEP estimates (I3/10-A3). The LWP of 24 g m^{-2} after spinup is similar to the value of 21.5 g m^{-2} reported by P98. Both IWP and SWP remain nearly constant after they reach their maximum values. The maximum IWP is about 30% of the value (6.2 g m^{-2}) reported by P98, while the maximum SWP is about 30% more than that (18.4 g m^{-2}) reported by P98 (Table 4, case 18.1). The differences in IWP and SWP between the modeled values and observations may be due to differences in categorization of hydrometeor in the model and in observations. A shorter-lived (lasts less than 1 h) stratus cloud with reduced LWP is produced when a weaker advective tendency is imposed (I3/10-A2). Of particular interest is that a pure liquid-phase stratus is simulated when the IFN is reduced further to 0.1 of its original value in the I1/10-A2 run. The LWP stays constant for about 10 min and then increases continuously for the rest of the simulation. Both IWP and SWP are practically zero because fewer ice crystals compete for the available water vapor and those that formed grew rapidly and precipitated. Consequently, all the water vapor available is converted to liquid water by condensation. The results of I1/10-A2 are not realistic since snow and ice were observed. This suggests that the stability of mixed-phase stratus is sensitive to the concentration of ice crystals or IFN.

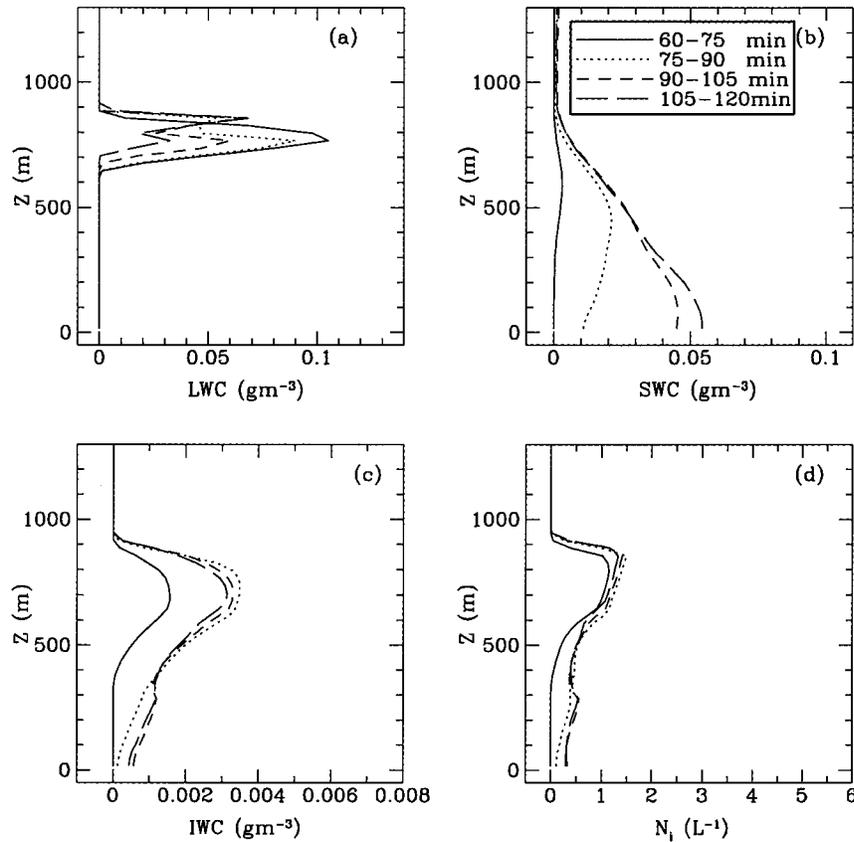The vertical profiles of LWC, IWC, SWC, and ice

FIG. 4. Domain-averaged vertical profiles of (a) LWC (g m^{-3}), (b) SWC (g m^{-3}), (c) IWC (g m^{-3}), and (d) ice crystal concentration (N_i) (L^{-1}) for the I3/10-A3 run. Solid line denotes average between 60 and 75 min, dotted line denotes between 75 and 90 min, short-dashed line denotes 90 and 105 min, and long-dashed line denotes between 105 and 120 min of simulation.

crystal concentration (N_i) from the most realistic simulation (I3/10-A3) and observations (mean plus standard deviation computed from legs flown at six heights, see P98 for flight pattern definition) are plotted (Figs. 4 and 5) to examine the temporal as well as spatial variations. The modeled fields are domain averaged and time averaged at 15-min blocks during the second hour of simulation.

The liquid and ice coexist throughout the entire second hour of the simulation (Figs. 4a and 4c). Note that the maximum LWC decreases from about 0.11 (solid line) to 0.07 g m^{-3} (long dashed line) during the 1-h time period. The trend of reducing LWC is clearly shown in the observed profiles 18.1 and 18.4 (Fig. 5a), which are taken within 50 km of each other and 3 h apart during the observation (see Table 1). The observed maximum LWC (direct measure of liquid water content made with the King probe) decreases from about 0.13 (case 18.1) to 0.05 g m^{-3} (case 18.4) during the 3-h time period. The vertical distributions of LWC agrees very well between Figs. 4a (I3/10-3A) and 5a (obs). Rauber and Tokay (1991) attributed the maintenance of a layer of supercooled water at cloud top to an imbalance between the condensation rate and the production rate

of ice in ascending air. They found that a supercooled layer could be maintained if ice crystals were small and particle concentrations are sufficiently low in this layer. The ice (Fig. 4c) is continuously produced at the expense of liquid water and subsequently removed to the subcloud layer, while IWC maintains a quasi-constant vertical profile. The N_i is about 1.5 L^{-1} in the cloud layer (Fig. 4d), and much smaller in the subcloud layer. The maximum SWC is initially located in the cloud layer but moved to the surface rapidly by sedimentation. Steady amounts of SWC are produced during the second half-hour of simulation. Overall a balance between the ice production, snow production, and condensation is maintained. H99 found that removal of ice crystals during the rapid glaciation phase are crucial to the stability of mixed-phase stratus clouds. The timescale required for the removal of ice from the cloud layer before cloud collapse in the sensitivity test of H99 is about 30 min. The timescale shown here is about the same.

The observed IWC and N_i are obtained by integrating over diameters from 50 to 250 μm in cloud and from 25 to 250 μm below cloud, while SWC is obtained by integrating over diameters from 250 to 3000 μm. Note that few particles are observed to be greater than 3 mm.
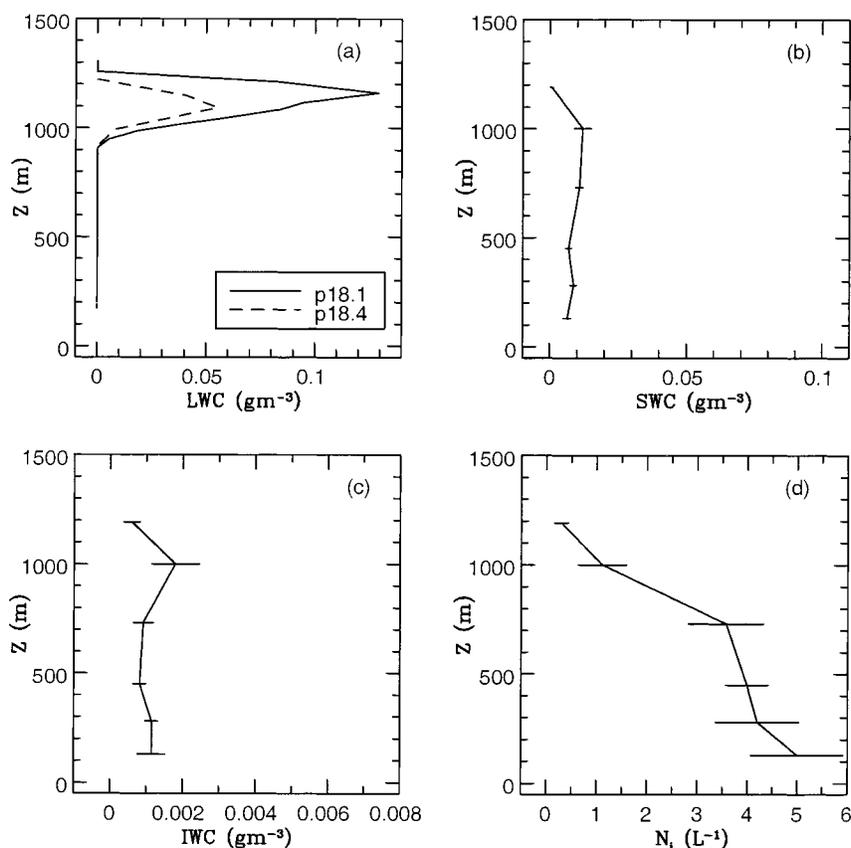
FIG. 5. Observed vertical profiles of (a) LWC (g m^{-3}) (case 18.1 and case 18.4), (b) SWC (g m^{-3}), (c) IWC (g m^{-3}), and (d) ice crystal concentration (N_i) (L^{-1}) (from P98 leg averages). The horizontal bars denote the standard deviations.

The average IWC (Fig. 5c) is about 0.001 g m^{-3} with the maximum of 0.002 g m^{-3} located near the liquid layer. The maximum observed IWC (Fig. 5c) is about 50% less than the maximum modeled value (Fig. 4c). Here N_i (Fig. 5d) decreases with height from 5 L^{-1} near the surface to 1 L^{-1} near cloud top. The near cloud-top value (1 L^{-1}) is about the same as the modeled one (1.5 L^{-1}). Another notable feature is that the relatively large N_i below cloud base is not produced in the model. One possibility is that the rapid conversion from ice to snow particles and subsequently fallout of the latter has effectively reduced the concentrations of ice crystals in the model.

A persistent stratus cloud layer is produced by reducing the ice concentration to three-tenths of the estimated value based on the midlatitude-derived formula (M92). P98 suggested that snowfall may effectively remove aerosols and result in the depletion of IFN in the Arctic environment, while Bigg (1996) argues that with the possible exception of open water regions, there are few sources of IFN. It is apparent that removing ice crystals through sedimentation is crucial to the stability of the stratus layer.

The concentration of IFN may be inferred indirectly

from measurements of condensation nuclei (CN) and other aerosols. Particle concentrations detected by the Passive Cavity Aerosol Spectrometer (PCAS) probe and the TSI CN counter during BASE (Fig. 6) indicate that the atmosphere is very clean. The PCAS probe detects a subset of the particles (0.1–2.75 μm) detectable by the CN counter, which has a detection limit of 0.05 μm. The observed CN concentrations are generally less than 200 cm^{-3} whereas typical springtime values over the Beaufort Sea are greater than 300 cm^{-3} (Hudson et al. 1999). In addition to starting with a relatively clean atmosphere, scavenging by the cloud layer further reduces aerosol concentrations. Minimum concentrations in CN and PCAS data are seen in clouds where nucleation scavenging has occurred. Below cloud base the CN decrease toward the surface indicating that the surface is not a source of CN and that the CN are likely being removed by snow, which is an efficient scavenger of aerosols. The production of IFN in the Arctic is limited as the surface is not a source of particles (e.g., clay, biogenic material) that serve as good IFN with the possible exception of open water leads where biogenic nuclei may be present (Schnell 1977). Since IFN, which are a very small subset of CN, are subject to similar
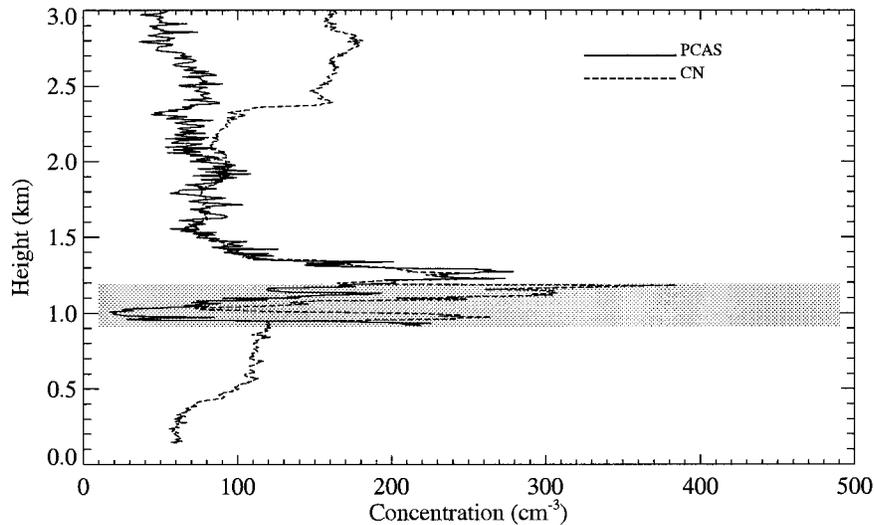
FIG. 6. Profiles of particle concentration obtained with the PCAS probe (solid line) and CN counter (dashed line) during an ascent made by the C-130 during flight 18. The cloudy region is shaded in gray. Data from the PCAS probe are suspect between 1 and 2 km. Below 1 km the PCAS data have been omitted due to poor quality.

processes and there are no nearby sources, it may be inferred that IFN are scarce.

Turbulent fluxes of $\langle w'w' \rangle$ and $\langle u'u' \rangle$ (not shown) for the most realistic simulation are also analyzed and compared with the observations. The maximum $\langle u'u' \rangle$ of 0.05 m^2 s^{-2} is similar in magnitude in the cloud layer, while it is slightly lower near the surface (0.06 m^2 s^{-2}), comparing with the observed values. The $\langle w'w' \rangle$ is only one-third of that observed (0.06 m^2 s^{-2}) in the cloud layer. However, the model failed to produce the maximum in $\langle w'w' \rangle$ near the surface as observed. Even with

a bin-resolving model, H99 did not produce the $\langle w'w' \rangle$ distributions similar to that reported in P98. We expect differences between the simulations and the observations to occur due to 1) use of a 2D framework, and 2) uncertainties in the specification of surface fluxes and/ or surface winds.

b. Sensitivity to large-scale advection

NCEP reanalysis showed that the advection varies substantially in the vertical and horizontal. In addition, estimates of horizontal advection from aircraft during BASE suggest that mesoscale variability can be quite large and may dominate the advective term locally (P98). Because of the relative absence of soundings in the Arctic, the advection terms derived from NCEP reanalysis contain a much greater degree of uncertainty than that estimated for more data-rich regions. Hence, we carry out sensitivity experiments to determine the importance of such uncertainties.

A similar plot as in Fig. 3 for the comparison among the I1-A1, I1-A2, I1-A3, and I1-A4 runs (Fig. 7) shows that the LWP is rapidly depleted from 23 g m^{-2} at the beginning of the second hour to zero 15 min later in the baseline (I1-A1) run. The average cloud liquid water for the first 25 min of hour 2 increases by 60% when the advective tendencies are doubled (I1-A2) and 150% when tendencies are quadrupled (I1-A4), while the simulated stratus cloud is going through rapid ice production at the expense of liquid water for all the runs. Only in the I1-A4 run is the large-scale advection of moisture significant and helps maintain a balance between condensation and precipitation, resulting in a tenuous layer of mixed-phase cloud.
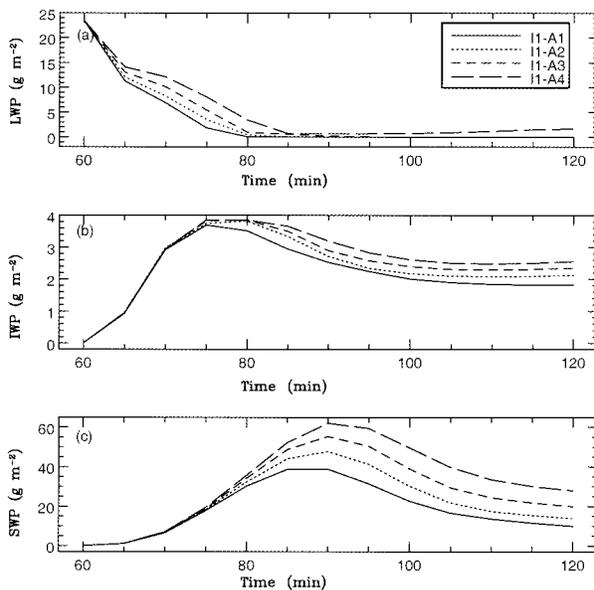

FIG. 7. Similar to Fig. 3 except comparison is among the I1-A1, I1-A2, I1-A3, and I1-A4 runs. See Table 2 for detail definitions.
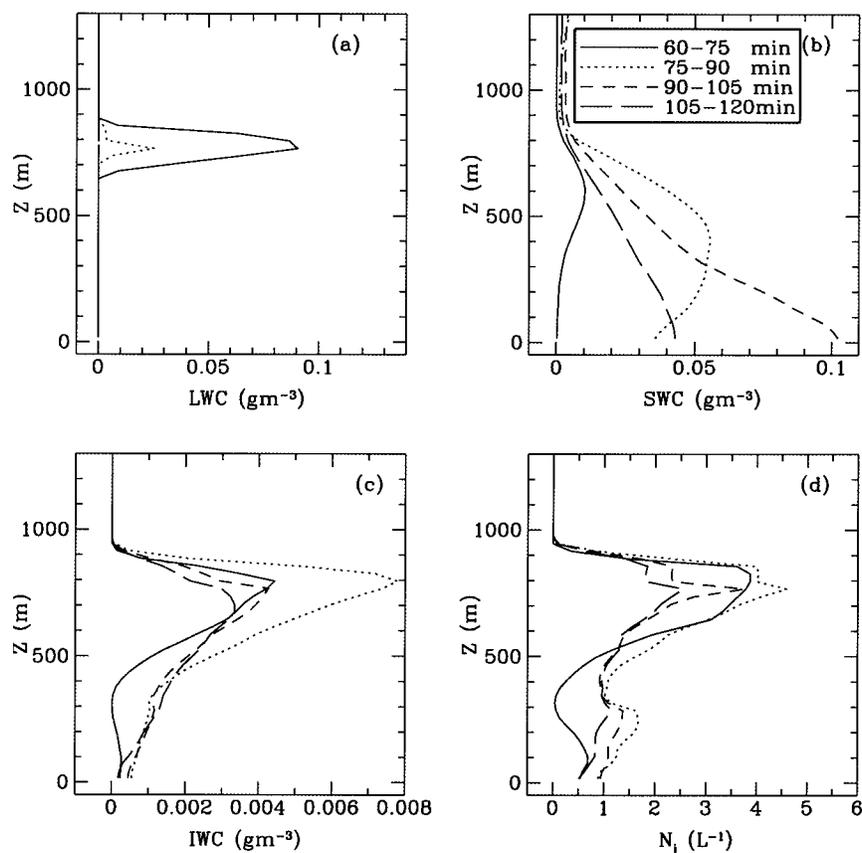
FIG. 8. Similar to Fig. 4 except for the I1-A3 run. See Fig. 4 caption for line-type definitions.

The IWP (Fig. 7b) increases very quickly to its maximum value of 4 g m^{-2} at the expense of liquid water within 15 min from the beginning of the second hour for all three runs, then decreases from 40% to 70% of its maximum value. The evolution of SWP lags that of IWP and reaches its maximum 15 min later, then decreases drastically to between 20% and 50% of its maximum by the end of the simulation. Higher values of IWP and SWP are produced in response to the increase in moisture and heat advection in each of the runs.

The vertical profiles of LWC, IWC, SWC, and N_i, a similar plot as in Fig. 4, for the I1-A3 run (Fig. 8) shows that LWC disappears completely from a value of 0.08 g m^{-3} after 20 min of simulation. IWC reaches its highest value for the average between 15 and 30 min. Thereafter, the production of ice water by deposition is balanced by the removal of ice water through sedimentation and snow production. The maximum SWC is initially located at cloud base (Fig. 8b, solid line) but shifts toward the surface with time. The N_i of 4.5 L^{-1} in the cloud layer is about three times that shown in Fig. 4d.

In the I1-A4 run (not shown), the mixed-phase cloud layer evolves with time in a similar manner as in the I1-A3 run except that a tenuous, mixed-phase stratus cloud with liquid layer depth of about 50 m is maintained after the majority of liquid water is converted to ice.

c. Impact on the surface energy budget

Curry et al. (1993) pointed out that variations in IFN composition and concentration may potentially affect the cloud microphysical and optical properties and surface radiative budgets. Thus factors of 2 or 3 variations in IFN concentrations in the Arctic may have substantial influence on the surface energy budget, effecting the freezing and melting of sea ice. This is illustrated in the temporal evolution of domain-averaged downwelling IR fluxes at the surface, F_I^- (Fig. 9). Here F_I^- (Fig. 9a) experiences a small, but steady increase during the second hour in both the I1/10-A2 run and I3/10-A3 run. The F_I^- in the I3/10-A2 run shows a similar trend except that it drops a significant amount after the liquid water is gone. In I1-A2 run, however, F_I^- has decreased about 50 W m^{-2} during a 40-min time period. The biggest difference in F_I^- is about 55 W m^{-2} between the I3/10-A3 and I1-A2 run.

The downward IR fluxes at the surface are also plotted as a function of large-scale advective tendencies in Fig. 9b to examine the sensitivity of the simulated stratus to
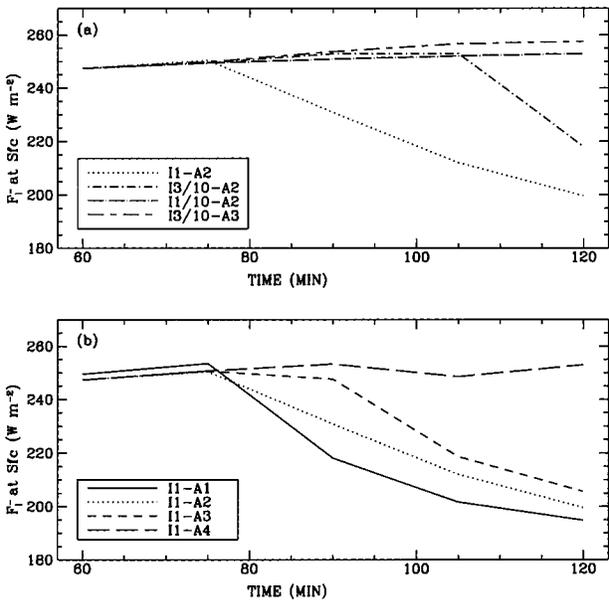
FIG. 9. Time evolution of surface downwelling IR radiative flux (W m^{-2}) (a) for the I1-A2, I3/10-A2, I1/10-A2, and I3/10-A3 runs, and (b) for the I1-A1, I1-A2, I1-A3, and I1-A4 runs, respectively.
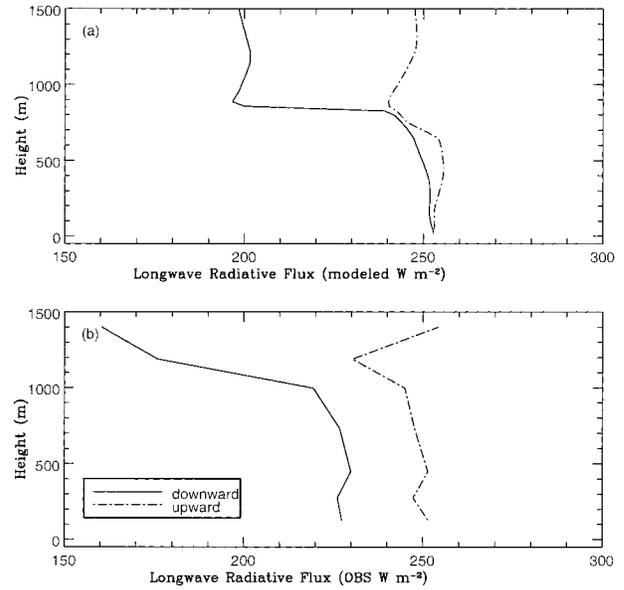

FIG. 10. Domain-averaged vertical profiles of upwelling and downwelling IR radiative flux (W m^{-2}) time averaged over the second hour of simulation for (a) I3/10-A3 run and (b) observed (leg average).

large-scale advection. The F_l^- from all the runs shown in Fig. 9b decreases with time at different rates except for the I1-A4 run, which remains nearly constant for the entire hour. The results shown in Fig. 9 suggest that the longwave radiative fluxes at the surface vary significantly depending on the modeled cloud phase.

The hourly averaged vertical profiles of upwelling and downwelling IR fluxes (F_l^-) (Fig. 10a) for the I3/10-A3 run compares reasonably well with the observational value (Fig. 10b), especially the upward flux. The modeled F_l^- is about 20 W m^{-2} higher than that observed.

Cloud-top radiative cooling (Fig. 11) exhibits a variation in response to the imposed large-scale advection as well as the concentration of ice crystals in the sensitivity experiments listed in Table 2. The maximum IR cooling at the cloud top increases from -15 to -40 K day^{-1} in response to the change in the magnitude of large-scale advection (Fig. 11, upper panels), and it varies from -55 to -90 K day^{-1} in response to the changes in both concentration of ice crystals and large-scale advection (Fig. 11, lower panels). Note that there is about -2 K day^{-1} cooling below the cloud layer in the I1-A2 (see label in the figure) and I1-A3 run, both of which experience the complete depletion of liquid water within a 15-min period during the second hour of simulation. Significantly stronger cloud-top cooling is associated with the persistent, mixed-phase stratus (I3/10-A3). The -90 K day^{-1} cooling compares well with the cooling rate of -95 K day^{-1} determined by P98 (Fig. 15) using observed cloud properties and a narrowband two-stream radiative transfer model. Solar ra-

diation in the fall is not significant due to the large solar zenith angle.

5. Summary

In this study we have examined how variations in ice crystal concentrations associated with variations in IFN alter the stability and structure of low-level Arctic stratus in a two-dimensional cloud resolving simulation. Data collected during BASE are used to initialize the model and subsequently used to test the model results against observations.

Using 30% IFN concentrations predicted by the Meyers et al. (1992) formula and increasing the large-scale advection by a factor of 3 results in a realistic mixed-phase cloud layer that is very similar to that reported by P98. This suggests that the concentrations of IFN in this case are relatively lower than those predicted by the Meyers et al. (1992). Bigg (1996) found that IFN concentration in the Arctic were one to two orders of magnitude lower than that found at lower latitudes. Sensitivity studies demonstrated that a variation of a factor of 2–3 in IFN concentrations can have a large impact on the evolution of the cloud microphysical structure and cloud phase. The large changes in cloud microphysics in turn have an important impact on the surface energy budget by affecting the downwelling radiative fluxes. The sensitivity studies for this case indicated potential variation in the downward longwave flux of over 55 W m^{-2} with the largest downward longwave fluxes being obtained for the case in which a solid mixed-phase cloud was maintained. Such changes in the
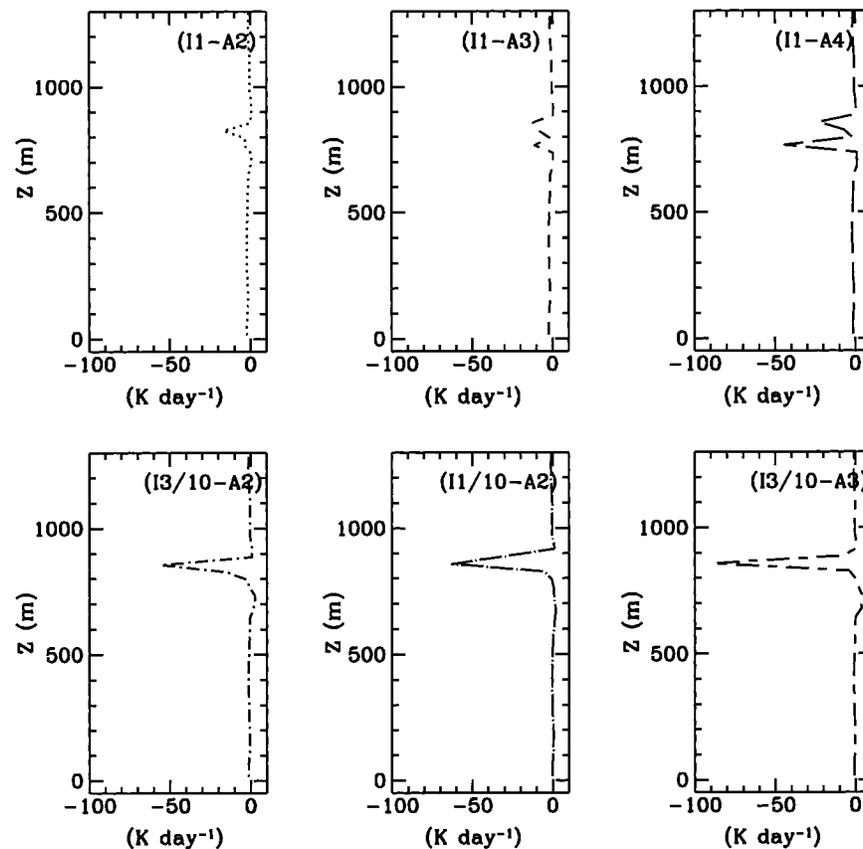
FIG. 11. Domain-averaged vertical profiles of longwave radiative cooling (K day^{-1}) averaged over the second hour of simulation for the I1-A2, I1-A3, I1-A4, I3/10-A2, I1/10-A2, and I3/10-A3 runs, respectively.

radiative energy budget at the surface can have important climatic affects by altering the melting and freezing rate of the Arctic ice pack during the transition seasons.

Furthermore, in the most realistic simulation, the imposed large-scale temperature and moisture advection is much greater than that estimated from the NCEP analysis. This suggests that direct measurements of advection on the mesoscale are needed for unambiguous evaluation of cloud resolving models over the Arctic. Most importantly, we have found that during the fall transition season[3] the simulated cloud is very sensitive to concentrations of ice crystals and, perhaps, the variability of IFN concentrations.

This work suggests that transition-season arctic stratus may be very vulnerable to anthropogenic sources of IFN and that such sources can affect the surface energy budget, thus reducing the melting rate and increasing the freezing rate of the arctic ice pack. Additionally, the

possibility of a marine source of IFN for the Arctic suggests a seasonal cycle to ice crystal concentration and mixed-phase clouds, which may be modulated by variations in sea ice extent and the amount of open water in leads.

In our most realistic simulation (I3/10-A3 run), which resulted from reducing IFN concentration, the concentrations of ice crystals, cloud-top temperature, LWC, and effective cloud particle radius are all similar to the averaged values in the April cases observed by HR98. The liquid droplets of 3–11 μm (Fig. 12) in diameter do not grow to the sizes that may initiate collision–coalescence processes. In their idealized simulation that resembled this case to quite an extent, H99 found that almost all of the ice was produced through vapor deposition and collision–coalescence processes had a very small impact on the stability of the mixed-phase cloud layer.

Nonetheless, there is evidence from HR98's observations over the Beaufort Sea that broad droplet spectra and drizzle formation does occur in arctic stratus and that the presence of such broad drop spectra can result in enhanced concentrations of ice crystals, perhaps by the Hallett–Mossop rime–splintering process. A ques-

---

[3] The spring case has yet to be tested with our numerical experiment, but based on the prevailing occurrence of the mixed-phase clouds during spring (Curry et al. 1990), we can infer that a similar behavior will be produced.
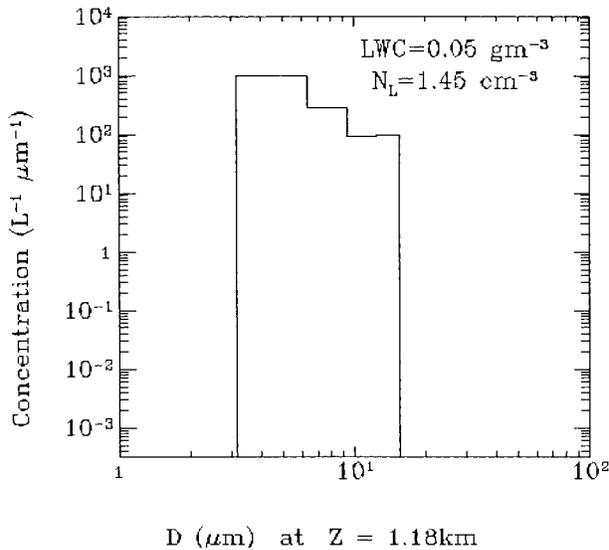
FIG. 12. Composite of liquid particle size distributions at $z = 1175$ m for case 18.1 from observations.

tion unanswered at the present is just how common are the conditions supporting a rime–splintering process in the Arctic? However, evidence that ice multiplication processes do not operate in arctic status clouds can be found in observations during spring (e.g., HR98), summer (e.g., Herman and Curry 1984), and fall (e.g., P98) seasons. Conclusions drawn from this case study apply to those mixed-phase arctic stratus clouds wherein riming–splintering does not operate.

One must also recognize that the presence of drizzle drops in Arctic stratus clouds has other implications to their dynamical characteristics. The removal of liquid water by drizzle will deplete the supercooled liquid layer near cloud top, and thus reduce cloud-top radiative cooling, weakening updrafts/downdrafts in the cloud (Chen and Cotton 1987) and possibly the collapse of the cloud layer (Ackerman et al. 1993) much like we find the ice phase does. Moreover, the evaporation of drizzle in the subcloud layer can alter the stability in the subcloud layer (Brost et al. 1982) leading to decoupling from the surface fluxes in some cases (Nicholls 1987), and at least with strong surface fluxes, a transition to a cumulus-under-stratus cloud regime (Stevens et al. 1998). Because the production of drizzle drops is highly dependent upon the concentration of CCN (e.g., H99), CCN concentration could play as important a role as IFN in determining the stability of mixed-phase clouds in the Arctic.

REFERENCES

Ackerman, A. S., O. B. Toon, and P. V. Hobbs, 1993: Dissipation of marine stratiform clouds and collapse of the marine boundary layer due to the depletion of cloud condensation nuclei by clouds. *Science,* **262,** 226–229.

Bigg, E. K., 1996: Ice forming nuclei in the high Arctic. *Tellus,* **48B,** 223–233.

Borys, R. D., 1989: Studies of ice nucleation by arctic aerosol on AGASP-II. *J. Atmos. Chem.,* **9,** 169–185.

Brost, R. A., J. C. Wyngaard, and D. H. Lenschow, 1982: Marine stratocumulus layers. Part II: Turbulence budgets. *J. Atmos. Sci.,* **39,** 818–836.

Chen, C., and W. R. Cotton, 1987: The physics of the marine stratocumulus-capped mixed layer. *J. Atmos. Sci.,* **44,** 2951–2977.

Curry, J. A., and E. E. Ebert, 1992: Annual cycle of radiation fluxes over the Arctic Ocean: Sensitivity to cloud optical properties. *J. Climate,* **5,** 1267–1280.

——, ——, and G. F. Herman, 1988: Mean and turbulent structure of the summertime Arctic cloudy boundary layer. *Quart. J. Roy. Meteor. Soc.,* **114,** 715–746.

——, F. G. Meyer, L. F. Radke, C. A. Brock, and E. E. Ebert, 1990: Occurrence and characteristics of lower tropospheric ice crystals in the Arctic. *Int. J. Climatol.,* **10,** 749–764.

——, J. L. Schramm, and E. E. Ebert, 1993: Impact of clouds on the surface radiation balance of the Arctic Ocean. *Meteor. Atmos. Phys.,* **51,** 197–217.

——, D. Randall, W. B. Rossow, and J. L. Schramm, 1996: Overview of Arctic cloud and radiation characteristics. *J. Climate,* **9,** 1731–1764.

——, J. O. Pinto, T. Benner, and M. Tschudi, 1997: Evolution of the cloudy boundary layer during the autumnal freezing of the Beaufort sea. *J. Geophys. Res.,* **102** (D12), 13 851–13 860.

Gregory, D., and D. Morris, 1996: The sensitivity of climate simulations to the specification of mixed phase clouds. *Climate Dyn.,* **12,** 641–651.

Harrington, J. Y., T. Reisin, W. R. Cotton, and S. M. Kreidenweis, 1999: Cloud resolving simulations of Arctic stratus. Part II: Transition-season clouds. *Atmos. Res.,* **51,** 45–75.

Herman, G. F., and J. A. Curry, 1984: Observational and theoretical studies of solar radiation in Arctic stratus clouds. *J. Climate Appl. Meteor.,* **23,** 5–24.

Hobbs, P. V., and A. L. Rangno, 1998: Microstructures of low and middle-level clouds over the Beaufort sea. *Quart. J. Roy. Meteor. Soc.,* **124,** 2035–2071.

Hudson, J. G., Y. Xie, and S. S. Yum, 1999: Spatial distribution of cloud condensation nuclei spectra in the spring Arctic. Preprints, *Fifth Conf. on Polar Meteorology and Oceanography,* Dallas, TX, Amer. Meteor. Soc., 200–201.

Kosovic, B., 1997: Subgrid-scale modeling for the large-eddy simulation of high-Reynolds-number boundary layers. *J. Fluid Mech.,* **336,** 151–182.

Kumai, M., and K. E. Francis, 1962: Nuclei in snow and ice crystals on the Greenland ice cap under natural and artificially simulated condition. *J. Atmos. Sci.,* **19,** 474–481.

Louis, J. F., 1979: A parameteric model of vertical eddy fluxes in the atmosphere. *Bound.-Layer Meteor.,* **17,** 187–202.

Meyers, M. P., P. J. DeMott, and W. R. Cotton, 1992: New primary ice-nucleation parameterizations in an explicit cloud model. *J. Appl. Meteor.,* **31,** 708–721.

Mitchell, D. L., A. Macke, and Y. Liu, 1996: Modeling cirrus clouds. Part II: Treatment of radiative properties. *J. Atmos. Sci.,* **53,** 2967–2988.

Mossop, S. C., 1985: Microphysical properties of supercooled cumulus clouds in which an ice particle multiplication process operated. *Quart. J. Roy. Meteor. Soc.,* **111,** 183–198.

Nicholls, S., 1987: A model of drizzle growth in warm, turbulent, stratiform clouds. *Quart. J. Roy. Meteor. Soc.,* **113,** 1141–1170.

Pinto, J. O., 1998: Autumnal mixed-phase cloudy boundary layers in the Arctic. *J. Atmos. Sci.,* **55,** 2016–2038.

Rauber, R. M., and A. Tokay, 1991: An explanation for the existence of supercooled water at the top of cold clouds. *J. Atmos. Sci.,* **48,** 1005–1023.

Ritter, B., and J.-F. Geleyn, 1992: A comprehensive radiation scheme for numerical weather prediction models with potential applications in climate simulations. *Mon. Wea. Rev.,* **120,** 303–325.

Schnell, R. C., 1977: Ice nuclei in seawater, fog water and marine air off the coast of Nova Scotia: Summer 1975. *J. Atmos. Sci.,* **34,** 1299–1305.

Slingo, A., and H. M. Schrecker, 1982: On the shortwave properties of stratiform water clouds. *Quart. J. Roy. Meteor. Soc.,* **108,** 407–426.

Smagorinsky, J., 1963: General circulation experiments with the primitive equations. *Mon. Wea. Rev.,* **91,** 99–164.

Stevens, B., W. R. Cotton, and G. Feingold, 1996: Equilibrium states in drizzling versus non-drizzling stratocumulus. Preprints, *12th Int. Conf. on Clouds and Precipitation,* Zurich, Switzerland, ICCP, 729–732.

——, ——, ——, and C.-H. Moeng, 1998: Large eddy simulations of strongly precipitating, shallow, stratocumulus-topped boundary layers. *J. Atmos. Sci.,* **55,** 3616–3638.

Tripoli, G. J., and W. R. Cotton, 1981: The use of ice-liquid water potential temperature as a thermodynamic variable in deep atmospheric models. *Mon. Wea. Rev.,* **109,** 1094–1102.

Walko, R. L., W. R. Cotton, M. P. Meyers, and J. Y. Harrington, 1995: New RAMS cloud microphysics parameterization. Part I: The single-moment scheme. *Atmos. Res.,* **38,** 29–62.